Electronic and magnetic properties of many-electron complexes in charged InAs$_x$P$_{1-x}$ quantum dots in InP nanowires

Jacob Manalo [1], Moritz Cygorek [1,2] Abdulmenaf Altintas [1], and Pawel Hawrylak[1]

[1]*University of Ottawa, Ottawa, Canada K1N 6N5*
[2]*Heriot-Watt University, Edinburgh EH14 4AS, United Kingdom*

We present here a microscopic theory of electronic complexes in charged InAs$_x$P$_{1-x}$ quantum dots in InP nanowires with a hexagonal cross section and determine the potential use of an array of such quantum dots as a synthetic spin chain for the possible construction of a topological qubit. The single-particle energies and wave functions are obtained by diagonalizing a microscopic atomistic tight-binding Hamiltonian of multiple quantum dots in the basis of $sp^3d^5s^*$ local atomic orbitals for a given random distribution of arsenic (As) vs phosphorus (P) atoms. The conduction band electronic states are found grouped into s, p, and d quantum dot shells. For a double dot, the electronic shells can be understood in terms of interdot tunneling despite the random distribution of As atoms in each quantum dot. The single- and double-dot structures were charged with a finite number of electrons. The many-body Hamiltonian including Coulomb electron-electron interactions was constructed using single atomistic particle states and then diagonalized in the space of many-electron configurations. For a single dot filled with $N_e = 1$–7 electrons, the ground state of a half-filled p-shell configuration with $N_e = 4$ was found with total electronic spin $S = 1$. The low-energy spectrum obtained using exact diagonalization of a Hamiltonian of a charged double dot filled with $N_e = 8$ electrons, i.e., half-filled p shells in each dot, was successfully fitted to the Hubbard-Kanamori and antiferromagnetic Heisenberg spin-1 Hamiltonians. The atomistic simulation confirmed the potential of InAsP/InP quantum dots in a nanowire for the design of synthetic spin chains.

I. INTRODUCTION

There is currently interest in designing quantum systems for quantum technologies, including quantum computation and quantum communication. This includes semiconductor quantum dots containing single- and multiple-electron complexes, with quantum information embedded in electron spin or encoded in multielectron configurations [1–15]. The single and double quantum dots have also been explored for the generation of single and entangled photon states [16–18], photon cluster states [19], lasers [20–22], and quantum dot photodetectors [23,24].

Here we focus on designing synthetic spin-1 chains using many-electron complexes in arrays of quantum dots embedded in semiconductor nanowires [10,25,26]. Many-electron complexes in self-assembled [26–30] and etched quantum dots [31,32] have already been extensively investigated. Here we discuss InAsP quantum dots in InP nanowires [17,25,26,33,34]. The electronic properties of these quantum dots can be designed by controlling the position, size, height, and arsenic concentration. The dots have a hexagonal disk geometry and are grown without a wetting layer using vapor-liquid-solid epitaxy, with a relatively low concentration of arsenic atoms replacing the phosphorus atoms [35]. As is the case with self-assembled dots, these dots suffer from intrinsic atomistic disorder. Despite the disorder, the conduction band states form electronic shells [34] that strongly resemble harmonic oscillator states observed in self-assembled quantum

dots [36–38]. The effect of disorder results in the effective quantum dot lateral anisotropy and plays a role in the removal of degeneracies of electronic shells. When engineering the total spin of the many-electron complexes, the degeneracies play an important role which leads to maximal spin at half-filled shells. Here we show that the spin-1 ground state survives atomistic disorder and that the different realizations of disorder on two vertically coupled quantum dots can be still understood in terms of interdot tunneling and the formation of bonding and antibonding electronic states. The many-electron complexes corresponding to half-filled p shells can be understood in terms of Hubbard-Kanamori and antiferromagnetic Heisenberg Hamiltonians for coupled spin-1 particles.

The problem of many-electron complexes in vertically coupled quantum dots has already been investigated using the effective mass model where atomic disorder was neglected and the Coulomb interactions were derived microscopically [10,31,39–41]. The atomistic description of an InAsP quantum dot in an InP nanowire and the many-exciton complexes were previously analyzed by Zielinski [42] and by some of us [34,43–45].

Here, we use a realistic tight-binding model consisting of millions of atoms with twenty ($spds^*$) orbitals each to compute the single-particle states, with strain, and the configuration interaction method to compute the many-body states of $N_e = 1 - 8$ electrons in single and double vertically coupled InAs$_x$P$_{1-x}$ quantum dots in an InP nanowire in the wurtzite phase.

We demonstrate that a single quantum dot containing $N_e = 4$ electrons in a half-filled p-shell configuration corresponds to a spin-1 ground state. Consequently, a chain of two vertically coupled quantum dots, each with a half-filled p shell, was found to have a low-energy electronic spectrum that resembles two antiferromagnetically coupled spin-1 particles. The atomistic disorder in the dots leads to a variation of tunneling matrix elements and spin-spin exchange coupling constants. The microscopic theory was later used to obtain parameters of a simplified Hubbard-Kanamori and a Heisenberg Hamiltonian. The Hubbard-Kanamori parameters obtained from atomistic calculations enable the description of larger chains and thus the investigation of a synthetic spin-1 Haldane material.

The paper is organized as follows. First, we briefly discuss the tight-binding and configuration interaction methods that are used to simulate the electronic properties of the quantum dots. We then describe the electronic properties of electronic complexes in a single InAs quantum dot in an InP nanowire, where we discuss the single-particle and many-body electronic states, and determine the spin of the ground state of the half-filled p shell to be $S = 1$. Next, we provide an analysis of the electronic properties of electrons in two vertically coupled quantum dots. Similar to the analysis of a single quantum dot, here we determine whether two quantum dots with half-filled p shells behave as two coupled spin-1 particles. This is followed by a description of the effective Hubbard-Kanamori model. Here, we compare the results of the Hubbard-Kanamori model with the Heisenberg chain and the atomistic tight-binding plus configuration interaction microscopic models. Finally, we discuss the results of both the Hubbard-Kanamori and microscopic models in the context of a synthetic Heisenberg chain.

II. MICROSCOPIC THEORY OF CHARGED InAs$_x$P$_{1-x}$ QUANTUM DOTS IN InP NANOWIRES

The microscopic theory of charged InAsP quantum dots in InP nanowires begins with a definition of atomistic structure followed by the computation of strain, construction of an atomistic tight-binding Hamiltonian from *ab initio* methods, and obtaining the single-particle states and energy spectrum. This is followed by the computation of Coulomb matrix elements constructed with the tight-binding atomistic single-particle states. We next introduce N_e additional electrons and construct many-body configurations and their interaction Hamiltonian to obtain a many-body spectrum by exact diagonalization [34,43,44]. Analysis of the spectrum and electron configurations then leads to our understanding of the electronic and magnetic properties of these nanostructures.

The single-particle states of a single and a double InAs$_x$P$_{1-x}$ quantum dot embedded in an InP nanowire are expanded in terms of local atomic orbitals as

$$\langle \mathbf{r}|i\rangle = \sum_k \sum_\alpha C_{ik\alpha}\phi_\alpha(\mathbf{r} - \mathbf{R}_k), \quad (1)$$

where $\phi_\alpha(\mathbf{r} - \mathbf{R}_k)$, the orbital α of atom k at location $\mathbf{R}_k$, is assumed to have the form

$$\phi_\alpha(\mathbf{r}) = A r^a e^{-br} Y_l^m(\theta, \varphi)\chi_\sigma. \quad (2)$$

Each atomic orbital has a radial component which is approximated as a Slater orbital with material-dependent parameters a and b, a spherical harmonic Y angular component, spinor component χ_σ, and normalization constant A.

Next the tight-binding Hamiltonian in the basis of $N_{orb} = 20$ $sp^3d^5s^*$ local atomic orbitals is constructed as

$$H_{TB} = \sum_{i=1}^{N_a}\sum_{\alpha=1}^{N_{orb}} \varepsilon_{i\alpha} c_{i\alpha}^\dagger c_{i\alpha} + \sum_{i=1}^{N_a}\sum_{\alpha,\beta=1}^{N_{orb}} \lambda_{i\alpha\beta} c_{i\alpha}^\dagger c_{i\beta}$$
$$+ \sum_{i=1}^{N_a}\sum_{j=1}^{nn(i)}\sum_{\alpha,\beta=1}^{N_{orb}} t_{i\alpha j\beta} c_{i\alpha}^\dagger c_{j\beta}. \quad (3)$$

Here $\varepsilon_{i\alpha}$ is the on-site energy, the spin-orbit interaction is $\lambda_{i\alpha\beta}$, and the tunneling matrix element is $t_{i\alpha j\beta}$, whereby the Roman indices denote atom and Greek indices denote atomic orbital. The values of these tight-binding parameters for the InAsP quantum dot nanowires are taken directly from Ref. [34]. Determination of these parameters involves fitting (3) to an *ab initio* DFT-based band structure as discussed in detail in Refs. [34,44,45]. We next introduce N_e electrons into our quantum dot.

The behavior of multielectron complexes is described by the many-body Hamiltonian

$$H_{MB} = \sum_i E_i c_i^\dagger c_i + \frac{1}{2}\sum_{ijkl} \langle ij|V|kl\rangle c_i^\dagger c_j^\dagger c_k c_l, \quad (4)$$

where the indices i refer to single-particle states and $\langle ij|V|kl\rangle$ are the Coulomb matrix elements.

Since the nanostructures under investigation contain several millions of atoms, necessary approximations to the Coulomb matrix elements are made in order to maintain computational feasibility. First, only two center integrals are computed, i.e., integrals that only involve scattering of electrons on one or two atoms, and second, only on-site and long-range terms are included, where $\langle ij|V|kl\rangle = \langle ij|V^{OS}|kl\rangle + \langle ij|V^{LR}|kl\rangle$. The on-site terms, given by

$$\langle ij|V^{OS}|kl\rangle = \frac{e^2}{4\pi\epsilon_0\epsilon_{OS}}\sum_{a\in N_a}\sum_{\alpha,\beta,\gamma,\delta} C_{ia\alpha}^* C_{ja\beta}^* C_{ka\gamma} C_{la\delta}$$
$$\times \int \frac{\phi_\alpha^*(\mathbf{r}_1)\phi_\beta^*(\mathbf{r}_2)\phi_\gamma(\mathbf{r}_2)\phi_\delta(\mathbf{r}_1)}{|\mathbf{r}_1 - \mathbf{r}_2|} d^3 r_1 d^3 r_2, \quad (5)$$

only contain integrals corresponding to scattering of orbitals on a single atom a. Due to the dependence of the dielectric constant on distance [46,47], the on-site dielectric constant ϵ_{OS} is taken to be 1.

The other significant contributions to the total Coulomb matrix element are the long-range terms, given by

$$\langle ij|V^{LR}|kl\rangle = \frac{e^2}{4\pi\epsilon_0\epsilon_{LR}}\sum_a\sum_{b\neq a}\sum_{\alpha\beta} C_{ia\alpha}^* C_{jb\beta}^* C_{kb\beta} C_{la\alpha}$$
$$\times \frac{1}{|\mathbf{R}_a - \mathbf{R}_b|}, \quad (6)$$

where the electron-electron Coulomb interactions are screened by bulk dielectric constant ϵ_{LR}. Since the electrons
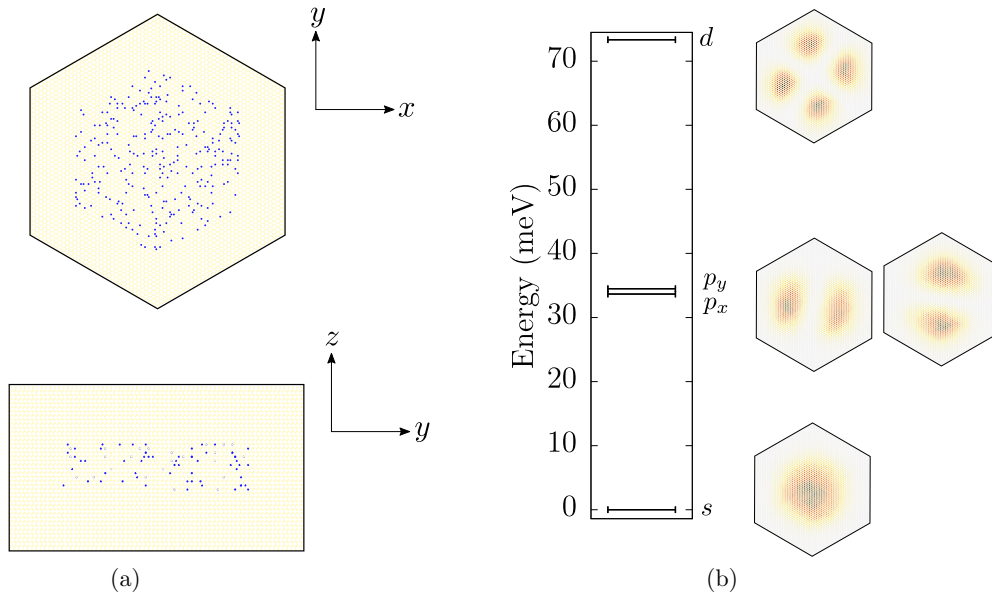
FIG. 1. (a) Top and side cross section of the quantum dot nanowire containing about 380 000 atoms. The diameter of the quantum dot is 18.2 nm and the thickness is 4.1 nm. The diameter of the nanowire is 28.2 nm and the height is 13.5 nm. (b) Single particle spectrum (left) and charge densities (right). The p_y charge density is located slightly higher than the p_x charge density to illustrate that the energy of the p_y state is slightly higher than the p_x energy.

located at atoms a and b are far apart, they can be treated as point charges which eliminates the need to compute the integrals explicitly. Furthermore, the only terms that survive the orthogonality relation between local atomic orbitals are terms where the atomic orbital angular momentum is conserved.

With the Coulomb matrix elements in place, the many-body states $|\nu\rangle$ of N_e electrons can be expanded in electronic configurations k as $|\nu\rangle = \sum_k A_k^\nu |k\rangle$. The many-body configurations, $|k\rangle = \prod_i c_i^\dagger |0\rangle$, are written as Slater determinants constructed from the finite number of single-particle orbitals i. Next, the matrix elements $\langle q|H|k\rangle$ of the many-body Hamiltonian are constructed in the space of configurations. The ground and excited states of the electronic complex are computed by diagonalization of the many-body Hamiltonian (4).

III. ELECTRONIC STATES OF A SINGLE InAs$_x$P$_{1-x}$ QUANTUM DOT IN InP NANOWIRE

A. Single-particle levels of a single InAs$_x$P$_{1-x}$ quantum dot in InP nanowire

Here we discuss the single-particle spectrum of a single quantum dot in a nanowire. We start with an InP nanowire and define a quantum dot volume. Within this volume we randomly replace P atoms with As atoms on the InP lattice, resulting in average concentration of As of 10%. The resulting strain is obtained by moving As atoms to minimize the total elastic energy. With the equilibrium position of atoms obtained, we construct a tight-binding Hamiltonian. Diagonalization of the tight-binding Hamiltonian (3) gives the single-particle spectrum of an InAs$_{0.1}$P$_{0.9}$InP quantum dot in an InP nanowire. Figure 1(a) shows the random distribution of the As atoms in the quantum dot. Despite this random distribution, the single-particle states, shown in Fig. 1(b), are grouped into s, p, and d quantum dot electronic shells, which are not to

be confused with the individual atomic orbitals as the quantum dot shells are localized throughout the whole quantum dot. However, due to the lateral asymmetry of the dot caused by random distribution of As atoms, the two states of the p shell, denoted as p_x and p_y, are not degenerate, but are split by an energy difference of $\Delta \approx 0.84$ meV. The splitting of the p shell is much smaller than the energy separation of different electronic shells, e.g., s-p and p-d shells with splitting of the order of 30 meV. Hence the p shell is approximately twofold degenerate as is the case with previously investigated effective mass models [14].

B. Many-electron complexes in a single InAs$_x$P$_{1-x}$ quantum dot in InP nanowire

We now turn to many-electron complexes in an InAs$_x$P$_{1-x}$ quantum dot in an InP nanowire. The many-body spectrum of an electronic complex is obtained through the diagonalization of the many-body Hamiltonian (4) in a basis consisting of all possible configurations built with a set of single-particle states. In this work, we retain 40 conduction band states. This basis already assured converged results for multiexciton states in a similar quantum dot [34]. For example, for $N_e = 4$ electrons with total spin $S = 0$ the Hilbert space consists of 85 048 configurations while for $S = 1$ we find 85 325 configurations. The overlap of the triplet configuration shown in Fig. 2 with the numerically obtained ground state is found to be high, with a value of 0.97. In Fig. 2 we show schematically configurations with significant overlap with the correlated ground state of the electron complexes consisting of $N_e = 1$–8 electrons.

C. Coulomb blockade spectroscopy

The many-body effects manifest themselves in the Coulomb blockade spectroscopy [2,7,25,48,49]. To determine the number of electrons N_e in the quantum dot and the effects
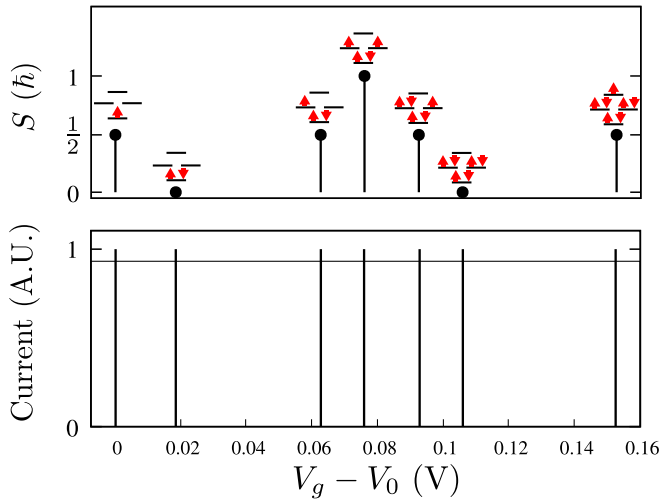
FIG. 2. Top: Total spin S for corresponding electronic complexes. Bottom: Coulomb blockade spectrum of many-body ground states as a function of relative back gate voltage where $V_0 = 1.483$ meV is the voltage corresponding to single-electron occupancy in the quantum dot, with chemical potential set at the top of the valence band.

of their interactions, source and drain leads can be attached and current can be measured as a function of back gate voltage V_g controlling the number of electrons in the quantum dot.

The current flows when the chemical potential of the quantum dot μ equals the chemical potential of the leads resulting in a Coulomb blockade spectrum [2,7]. Hence the Coulomb blockade spectrum as a function of back gate voltage directly measures the many-body N_e and $N_e - 1$ electron ground states, as

$$eV_g = E(N_e) - E(N_e - 1). \qquad (7)$$

We have computed the chemical potential of the quantum dot, the Coulomb blockade spectrum, for different electron numbers N_e. As shown in the Coulomb blockade spectrum of the single dot in Fig. 2, there are large gaps in between the second and third peaks and between the sixth and seventh peaks [25,27,32,49]. The first gap is due to the s-p shell energy splitting and the second large gap is due to the p-d shell energy splitting. The remaining variations in Coulomb blockade peaks reflect electronic interactions, both exchange and correlations, in degenerate shells [27].

Also shown in Fig. 2 is the total electronic spin S of the ground state as a function of V_g. The oscillatory behavior between $S = 0$ and $S = 1$ is indicative of Hund's rule being satisfied. It is shown in the Coulomb blockade spectrum (Fig. 2) that an $N_e = 4$ quantum dot with half-filled p shells generates a spin-1 ground state. Further analysis of the $N_e = 4$ half-filled p-shell spectrum is necessary in order to understand the electronic and magnetic properties of the InAsP quantum dot nanowire.

IV. ELECTRONIC AND MAGNETIC PROPERTIES OF A HALF-FILLED p SHELL

The evolution of the energy spectrum of the $N_e = 4$ complex in a single dot as a function of increasing number of

different electronic configurations is shown in Fig. 3. We start with two almost degenerate p_x, p_y orbitals. We place two electrons, one with spin up and one with spin down, onto the p shell as shown in Fig. 3(a). Next, we form a spin triplet configuration with $S_z = 0$, schematically shown here with both spins up, and a spin singlet configuration. The exchange interaction V_{ex} is then turned on. This lowers the energy of spin triplet configuration compared to singlet configuration by $2V_{ex}$, as shown in Fig. 3(b). Finally, we add two doubly occupied configurations, where two electrons, spin up and down, occupy either the p_x or p_y orbital as shown in Fig. 3(c).

We next turn on interaction among all singlet singly and doubly occupied configurations. The antisymmetric combination of doubly occupied configurations remains decoupled from other singlet configurations but a symmetric combination of doubly occupied configurations couples with singly occupied one. This lowers the energy of mostly doubly occupied configurations and increases the energy of mostly singly occupied configurations as shown in Fig. 3(d). For the doubly occupied singlet configuration, the doubly occupied configurations contribute 89% to the total wave function and the singly occupied configurations contribute about 6%. The remaining 5% comes from other contributions, such as ones where the d state is occupied. For the singly occupied singlet, contributions are interchanged, where 6% of the wave function comes from doubly occupied configurations and 89% comes from singly occupied configurations. So retaining only the singly and doubly occupied configurations on a p shell is a reasonable approximation. Finally, the gap Δ separating the triplet and singlet configurations is reduced from $\Delta = 2V_x$ to $\Delta = V_x - \delta$ where δ represents the correlation contribution. The important conclusion is that the triplet configuration remains the ground state of the $N_e = 4$ electron complex in accordance with Hund's rules. Since the ground state of a single quantum dot is shown to behave as a spin-1, the next step is to determine whether two quantum dots act as two coupled spin-1's.

V. MICROSCOPIC THEORY OF TWO COUPLED CHARGED InAs$_x$P$_{1-x}$ QUANTUM DOTS IN InP NANOWIRE

We now turn to two coupled charged InAs quantum dots in InP nanowire. The double-dot system consists of two quantum dots with the same dimensions and concentrations as the single quantum dot, with a diameter of 18.2 nm and a thickness of 4.1 nm. Cross sections of the two dots in a nanowire with an interdot distance of 5.4 nm are shown in Fig. 4(a). The lower panel shows the probability density of the s and two p orbitals. The z-y cross section (bottom panel) shows that the p orbitals on the two dots form molecular π bonds. This is due to the tunneling between the two dots which gives rise to eigenstates that are a linear combination of the local quantum dot orbitals [50]. This is seen more clearly if the dots are approximated as sites containing a local harmonic orbital (LHO) each, with $|B\rangle$ being the bottom dot orbital and $|T\rangle$ being the top dot orbital. If we assume the on-site energy is the same for both sites, then the Hamiltonian in the BT basis of p_x (p_y) orbitals is given by

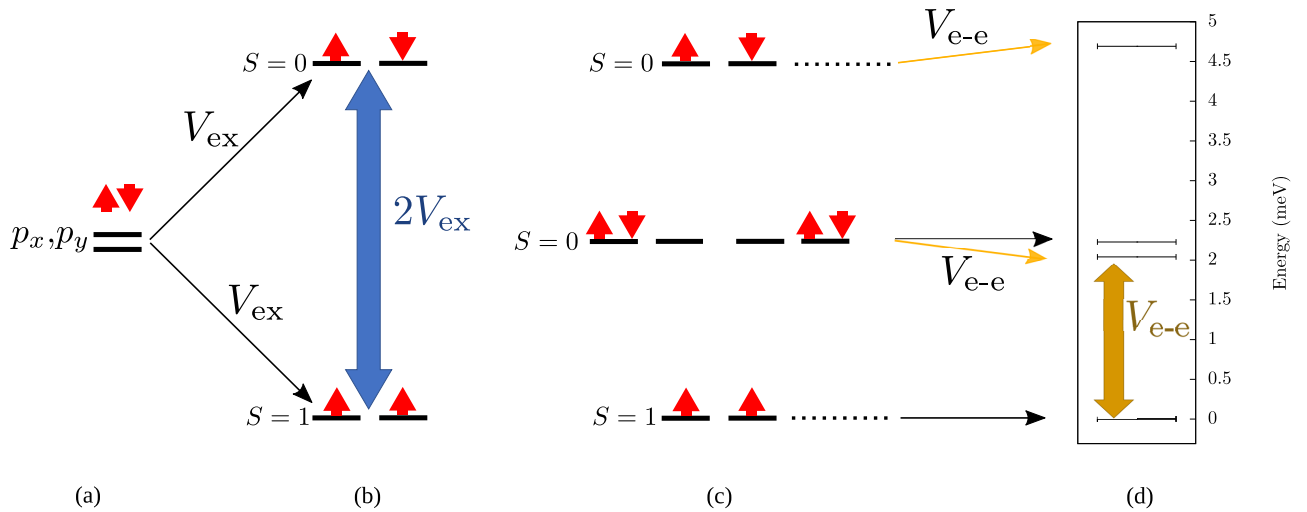$$H_{2-site} = \begin{bmatrix} 0 & -t \\ -t & 0 \end{bmatrix}, \qquad (8)$$

FIG. 3. (a) Schematic of configurations on the half-filled p shell. Two electrons occupy the p_x and p_y orbitals. (b) Schematic of the low-energy spectrum containing only singly occupied configurations. The ground state is a triplet and the excited state is a singlet. The splitting is twice the exchange energy V_x. (c) The low-energy spectrum including doubly occupied configurations. (d) The low-energy many-body spectrum from the atomistic simulation. The splitting between the ground state and first excited state is the Coulomb interaction energy V_{ee}.

where t is the tunneling matrix element mixing the two sites. The eigenstates are then symmetric $|S\rangle = \frac{1}{\sqrt{2}}(|T\rangle + |B\rangle)$ and antisymmetric $|AS\rangle = \frac{1}{\sqrt{2}}(|T\rangle - |B\rangle)$ linear combinations of T and B orbitals, with energies $-t$ and t, respectively. The symmetric-antisymmetric splitting is thus $2t$.
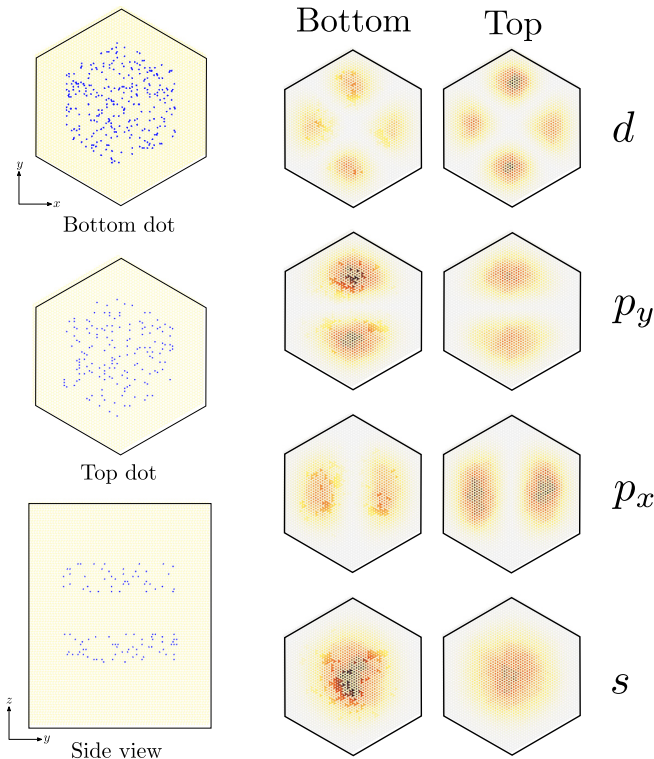

FIG. 4. (a) Cross sections of the double-dot nanowire structure containing about 435 000 atoms. The As atoms are blue and both the In and P atoms are yellow. (b) Charge densities of the single-particle states.

For the atomistic double quantum dot in a nanowire, the single-particle states come in symmetric-antisymmetric pairs as well, where each energy level is labeled with the corresponding orbital [39,51]. As is the case with the single-dot nanowire, the charge probability densities for the double dot exhibit s, p, and d symmetry as seen in Fig. 4(b). The tunneling strength for given orbitals on the two dots, which is half of the symmetric-antisymmetric energy splitting, decreases exponentially with respect to interdot distance. The tunneling matrix element for p-shell orbitals as a function of interdot distance is defined as $|t| = E_{A,p_x} - E_{S,p_x}$. Using the least-squares method, the tunneling matrix element dependence on interdot distance was obtained from atomistic energy splittings with an error of about $\chi^2 = 0.06$ meV^2. The exponential dependence of the tunneling strength on interdot distance allows for tuning of the tunneling matrix element. In addition to interdot tunneling, electron-electron interactions between the dots must be taken into account in order to understand the properties of the half-filled p-shell configuration of the double dot.

VI. ELECTRONIC AND MAGNETIC PROPERTIES OF TWO COUPLED InAs$_x$P$_{1-x}$ QUANTUM DOTS WITH HALF-FILLED p SHELL EACH

We now turn to the analysis of properties of two coupled quantum dots, each with the half-filled p-shell configuration. To do this we must diagonalize the many-body Hamiltonian (4) for $N_e = 8$ electrons where index i denotes single-particle eigenstates of the double-dot tight-binding Hamiltonian (3). We construct 76 904 685 possible $N_e = 8$ electron configurations on $N_c = 40$ single particle states and diagonalize the many-body Hamiltonian. The numerically obtained low-energy many-body spectrum $E(n)$ for $N_e = 8$ electrons in a double quantum dot nanowire is shown in Fig. 5.

We see that the lowest energy, $n = 0$, state with energy E_0 is nondegenerate and is the singlet state. The next in energy
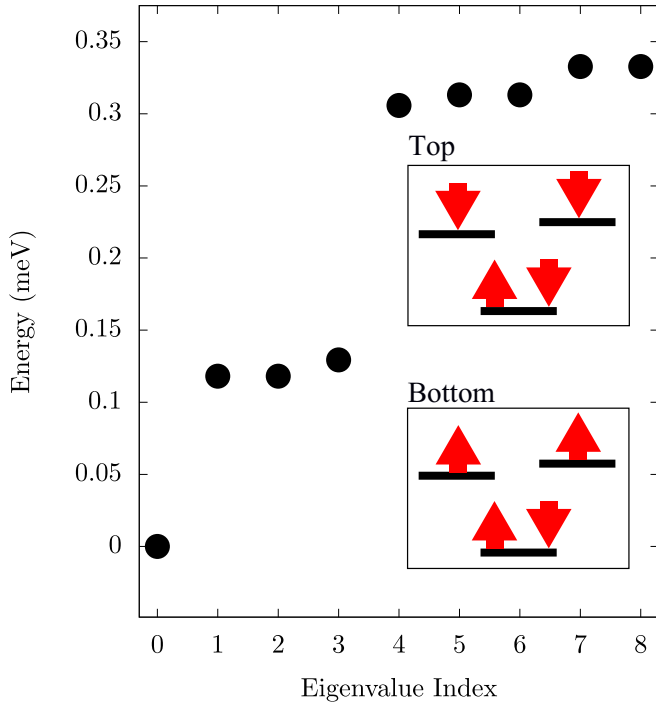
FIG. 5. Many-body spectrum of the 8-electron complex for a double quantum dot nanowire of 14.9 nm interdot distance. The inset shows schematic half-filled p-shell configurations on top and bottom quantum dots.

are the three states E_1–E_3 of an almost degenerate triplet followed by a quintuplet E_4–E_8 of almost degenerate states. This low-energy spectrum is identical to the spectrum of two spin-1's, S_1 and S_2, coupled by exchange interaction and described by the Heisenberg Hamiltonian $H = J_{AF}\vec{S}_1 \cdot \vec{S}_2$, where J_{AF} is the interdot antiferromagnetic exchange constant, which is discussed in further detail in the following section. The differences between the microscopic spectrum and that of a Heisenberg chain are due to small contributions from higher energy configurations, such as doubly occupied configurations and configurations that contain d-shell orbitals and higher. Such contributions are the largest for the quintuplet state. We now use the numerical spectrum of the $N_e = 8$ complex to obtain parameters for a simplified microscopic model, the Hubbard-Kanamori model.

VII. EFFECTIVE HUBBARD-KANAMORI MODEL

Though the many-body Hamiltonian, Eq. (4), provides an accurate description of the electronic complexes in up to 2 quantum dots in a nanowire it cannot be extended to a larger number of quantum dots with 4 electrons per dot. Hence we discuss the simplified Hubbard-Kanamori model capturing the essential features that might give rise to the behavior of a Heisenberg spin-1 chain. In this model, the s-shell electrons are frozen and we retain only two orbitals, p_+ and p_-, and two electrons on each quantum dot.

A. The Hubbard-Kanamori Hamiltonian

To derive the Hubbard-Kanamori Hamiltonian, we start with the many-body Hamiltonian written in the basis of

p_+ and p_- degenerate orbitals localized on each idealized, disorder-free quantum dot. The many-body Hamiltonian in this basis is given by

$$H_{MB} = \sum_{i,\alpha,\sigma} E_{i\alpha\sigma} c^\dagger_{i\alpha\sigma} c_{i\alpha\sigma} + \sum_\sigma \sum_{ij} \sum_{\alpha\beta} t_{i\alpha,j\beta} c^\dagger_{i\alpha\sigma} c_{j\beta\sigma}$$
$$+ \frac{1}{2} \sum_{\sigma\sigma'} \sum_{ijkl} \sum_{\alpha\beta\gamma\delta} \langle i\alpha, j\beta|V|k\delta, l\gamma\rangle c^\dagger_{i\alpha\sigma} c^\dagger_{j\beta\sigma'} c_{k\delta\sigma'} c_{l\gamma\sigma},$$
(9)

where the Roman indices i, j, k, and l denote quantum dot number, indices α, β, δ, and γ denote quantum dot orbitals p_+ or p_-, and σ denotes the electron spin. Here, the first term describes energies of degenerate p-shell orbitals, the second term describes interdot tunneling and intradot disorder, and the third term describes intra- and interdot electron-electron interactions. With the first term describing energies of two degenerate p orbitals, $t_{i\alpha,i\beta}$ describes mixing of p_+, p_- orbitals on the same dot i by the atomistic disorder, leading to an energy splitting Δ while $t_{i\alpha,i+1\alpha}$ describes tunneling of electron between p_+ (p_-) orbitals on neighboring dots. For two dots, this tunneling translates to the symmetric (antisymmetric) orbitals and energy splitting.

To simplify (9) further, all interdot and intradot tunneling matrix elements are written as

$$t_{i\alpha\sigma,i\beta\sigma} \equiv \frac{\Delta}{2},$$
(10)

$$t_{i\alpha\sigma,j\alpha\sigma} \equiv t,$$
(11)

for all i, α, β, and σ. Moreover, all of the other tunneling matrix elements are zero since all tunneling, intradot or interdot, conserves spin and interdot tunneling conserves orbital angular momentum.

In the spirit of the Hubbard-Kanamori model, similar approximations are made for the electron-electron interaction matrix elements, where the only nonzero matrix elements between nearest-neighboring dots 1 and 2 are

$$\langle 1\alpha, 1\beta|V|i\beta, 1\alpha\rangle = \langle 1\alpha, 1\alpha|V|1\alpha, 1\alpha\rangle \equiv U,$$
(12)

$$\langle 1\alpha, 1\beta|V|1\alpha, 1\beta\rangle \equiv \frac{J}{2},$$
(13)

$$\langle 1\alpha, 2\alpha|V|2\alpha, 1\alpha\rangle \equiv V,$$
(14)

$$\langle 1+, 2-|V|2+, 1-\rangle \equiv W.$$
(15)

Note the last Coulomb matrix element W conserves the total angular momentum of the electron pair but corresponds to scattering of electron pair from dot 1 to dot 2 with exchange of electrons. With all of these reductions, the many-body Hamiltonian (9) reduces to the Hubbard-Kanamori Hamiltonian for two dots given by

$$H = H_0(1) + H_0(2)$$
$$+ \sum_{\alpha\sigma} (t_{12} c^\dagger_{1\alpha\sigma} c_{2\alpha\sigma} + t_{12} c^\dagger_{2\alpha\sigma} c_{1\alpha\sigma})$$
$$+ V(n_{1,+} + n_{1,-})(n_{2,+} + n_{2,-})$$
$$+ W L_1^+ L_2^- + W^* L_1^- L_2^+,$$
(16)

where $H_0(1)$ is the Hubbard-Kanamori Hamiltonian for a single quantum dot

$$H_0 = \sum_{\alpha,\sigma} E_{\alpha,\sigma} n_{\alpha,\sigma} + \frac{\Delta}{2} \sum_{\sigma} \sum_{\alpha \neq \beta} c_{\alpha\sigma}^{\dagger} c_{\beta\sigma}$$
$$+ U n_{-\uparrow} n_{-\downarrow} + U n_{+\uparrow} n_{+\downarrow}$$
$$+ \left(U - \frac{J}{4} \right)(n_{-\uparrow} + n_{-\downarrow})(n_{+\uparrow} + n_{+\downarrow}) - J \mathbf{S}_- \cdot \mathbf{S}_+, \quad (17)$$

where $\alpha \in \{+, -\}$ labels the two degenerate orbitals p_-, p_+, $E_{\alpha,\sigma} = E$ are the energies of the two degenerate orbitals, and Δ describes mixing of p-shell orbitals by microscopic disorder and lattice effects, ferromagnetic exchange coupling J aligns the spins of two p-shell electrons, $n_i = n_{i,\uparrow} + n_{i,\downarrow}$ is the number of electrons on state with quantum number i, $S_{i\alpha}^+ = c_{i\alpha\uparrow}^{\dagger} c_{i\alpha\downarrow}$, $S_{i\alpha}^- = (S_{i\alpha}^+)^{\dagger}$, $S_{i\alpha}^z = \frac{1}{2}(c_{i\alpha\uparrow}^{\dagger} c_{i\alpha\uparrow} - c_{i\alpha\downarrow}^{\dagger} c_{i\alpha\downarrow})$, $L_i^+ = \sum_{\sigma} c_{i+\sigma}^{\dagger} c_{i-\sigma}$, and $L_i^- = (L_i^+)^{\dagger}$.

We note that while the tunneling of a single electron from one dot to another conserves the angular momentum, i.e., tunneling takes place between p_+ orbital on one dot to p_+ orbital on neighboring dot, the last term is a bit unusual; it involves tunneling of two electrons, one electron from the $p+$ orbital on one dot to the p_- orbital on the second dot simultaneous with second electron tunneling from the p_- orbital to p_+ orbital on a second dot. Hence the total angular momentum of the electron pair is conserved but electrons change orbitals in a scattering event. We also note the presence of ferromagnetic Heisenberg coupling J, which is the exchange interaction between two electrons on the p shell in the same quantum dot. The coupling of the two spins on dots 1 and 2 is described by the interdot tunneling and interactions. All the parameters entering the Hubbard-Kanamori Hamiltonian will be extracted from a microscopic model below.

B. Analysis of Hubbard-Kanamori model for a single quantum dot

The Hubbard-Kanamori spectrum of two electrons in a single dot is obtained by diagonalizing the Hamiltonian, (17), in the basis of L_z, S^2, and S^z simultaneous eigenstates constructed out of singly and doubly occupied two-electron configurations, with the spectrum identical to the one computed microscopically and shown in Fig. 3(d). The eigenvalues of the single-dot Hubbard-Kanamori Hamiltonian are $E_T = 2E$ for a threefold-degenerate triplet and three singlet states $E_{S1} = 2E + \frac{1}{4}[3J - \sqrt{J^2 + (4\Delta)^2}]$, $E_{S2} = 2E + \frac{J}{2}$, $E_{S3} = 2E + \frac{1}{4}[3J + \sqrt{J^2 + (4\Delta)^2}]$.

When the p-shell splitting is zero, the splitting between the triplets and the doubly occupied singlets is equal to the intrashell exchange J while the splitting J between 3 triplets and the singly occupied singlet is twice the exchange matrix element. When p-shell splitting Δ is nonzero, the degeneracy of the doubly occupied configurations is lifted and the singly occupied singlet increases in energy. This is due to the fact that the p-shell mixing couples one of the doubly occupied configurations to the singly occupied singlet. The triplet states remain uncoupled because p-shell mixing must conserve S and S^z. With the full energy spectrum expressed
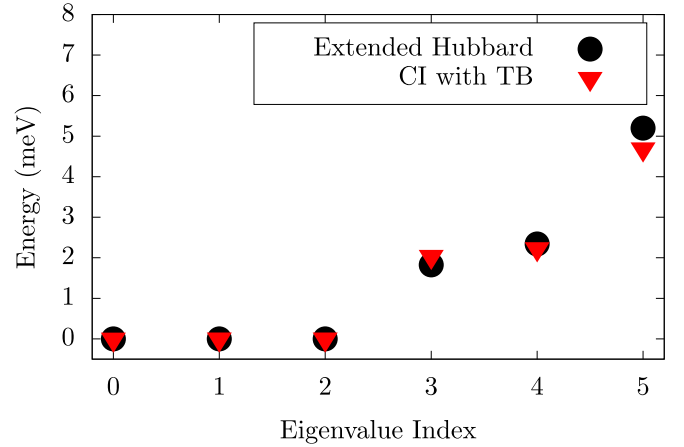

FIG. 6. Comparison between Hubbard-Kanamori and atomistic spectra.

in terms of the Hubbard-Kanamori parameters, fitting the Hubbard-Kanamori spectrum to the atomistic spectrum shown in Fig. 3(d) enables the extraction of Hubbard-Kanamori parameters. We find for the typical $InAs_xP_{1-x}$ quantum dots studied here $U = 16$ meV, $J = 5$ meV, and $\Delta = 0.8$ meV. For these parameters we show in Fig. 6 both the Hubbard-Kanamori spectrum and the full microscopic spectrum of 4 electrons on a single dot.

The Hubbard-Kanamori and atomistic spectra are in close agreement. The largest difference of 0.5 meV is in the energy of the singly occupied singlet. Just as in the atomistic spectrum, the ground state is the threefold-degenerate triplet, followed by two doubly occupied singlet states and a singly occupied singlet. As discussed before, the spin-polarized ground state can be understood in terms of the exchange coupling between the p-shell electrons as shown in Eq. (16). Having shown the correspondence between the Hubbard-Kanamori and atomistic models for a single quantum dot, we can now use these single quantum dot parameters in the double quantum dot Hubbard-Kanamori Hamiltonian to determine the double quantum dot spectrum for 4 electrons on two p shells.

C. Analysis of Hubbard-Kanamori model for a double quantum dot

Unlike in the single quantum dot, analytically determining the many-body spectrum for a double quantum dot consisting of 4 p-shell states and 4 active electrons would be difficult as the Hilbert space of the Hubbard-Kanamori model consists of 70 configurations. We hence fit the Hubbard-Kanamori spectrum, Eq. (16), to the atomistic spectra numerically. To better understand the effect of interdot tunneling and interactions on the double-dot spectrum we start with a double dot without tunneling and interactions. Assuming the two quantum dots are identical, we form eigenstates with 2 electrons on each p shell by forming products of many-body eigenstates between the two single quantum dots provided S and L are conserved. Examples of these eigenstates formed in this manner are the
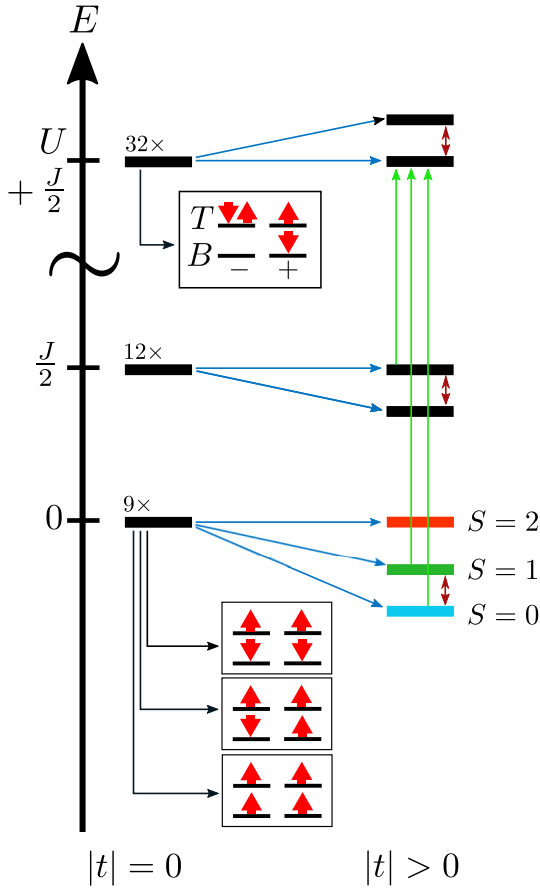
FIG. 7. Schematic energy spectrum of a double quantum dot. On the left is the double-dot spectrum when $t = 0$ and on the right is the spectrum when $|t| > 0$. The bottom insets show the configurations of one of terms of the $S^z = 0$ triplet as well as the $S^z = -1$ and $+1$ triplet states configurations. The top inset shows one of the configurations that contain three electrons in one dot. Blue arrows indicate splittings of levels due to tunneling. On the right, the green arrows indicate coupling between states due to tunneling. The red, green, and cyan states correspond to the singlet, triplet, and quintuplet states. The double-headed red arrows indicate a splitting of $\frac{2t^2}{U+J/2}$.

ground states of maximal S^z given by

$$|S_T = 0, S^z = 0\rangle = \alpha_s(|\downarrow\downarrow; \uparrow\uparrow\rangle + |\uparrow\uparrow; \downarrow\downarrow\rangle)$$
$$+ \beta_s(|\downarrow\uparrow; \uparrow\downarrow\rangle + |\downarrow\uparrow; \downarrow\uparrow\rangle$$
$$+ |\uparrow\downarrow; \downarrow\uparrow\rangle + |\uparrow\downarrow; \uparrow\downarrow\rangle)),$$
$$|S_T = 1, S^z = 1\rangle = \alpha_t(|\uparrow\uparrow; \uparrow\downarrow\rangle + |\uparrow\uparrow; \downarrow\uparrow\rangle$$
$$- |\uparrow\downarrow; \uparrow\uparrow\rangle - |\downarrow\uparrow; \uparrow\uparrow\rangle),$$
$$|S_T = 2, S^z = 2\rangle = \alpha_q|\uparrow\uparrow; \uparrow\uparrow\rangle. \quad (18)$$

Here we neglect eigenstates with triple and quadruple occupancy in a quantum dot. The energies of these configurations would be higher in energy by U. A schematic for the noninteracting Hubbard-Kanamori spectrum without tunneling and electron-electron interactions is shown in Fig. 7. The left-hand side shows the Hubbard-Kanamori spectrum of two noninteracting quantum dots with 2 electrons each. The spectrum is the same as a Hubbard-Kanamori spectrum of

TABLE I. Fitted Hubbard-Kanamori parameters for the double quantum dot nanowire.

Fitted H-K Parameter	Numerical Value (meV)
U	15.971
$\frac{J}{2}$	2.500
Δ	0.844
t	0.748
V	7.734
W	0.000

a single dot but degenerate. Hence the lowest energy band consists of 3 triplet states on each dot, with a total of 9 states.

The right-hand panel shows the energy spectrum of a double dot as interdot tunneling is turned on. We see that the singlet, triplet, and quintuplet states are no longer degenerate. This is due to the singlets and triplets coupling to the triply occupied configurations as shown in Fig. 7. The quintuplet states however remain uncoupled since tunneling conserves S. Most importantly, the singlet, triplet, and quintuplet degeneracies are lifted in a manner that resembles the spectrum of a Heisenberg chain of spin-1 particles with coupling $J_H = \frac{2t^2}{U+J/2-V}$. The reduction of the Hubbard-Kanamori Hamiltonian (16) to the Heisenberg spin-1 chain Hamiltonian is discussed in further detail in Ref. [52] where interdot tunneling is treated perturbatively. In essence, the behavior of coupled spin-1 spins arises when the ferromagnetic intradot coupling J between electrons on two different p-shell orbitals is much stronger than the interdot coupling between composite spin-1 particles (i.e., $J \gg J_H$). If J_H is large, then the tunneling is no longer a perturbation and the intradot coupling J is no longer strong enough to hold two electron spins parallel in a single quantum dot.

The Hubbard-Kanamori parameters for the double quantum dot are obtained in a manner similar to that for the single quantum dot system. First initial guesses are made by relating the parameters to the atomistic single-particle spectrum and Coulomb matrix elements. However, in the case of the double quantum dot, a genetic algorithm is used to make adjustments to the parameters to obtain an accurate fit to the microscopic many-body spectrum. The algorithm is as follows. First, random parameters are generated within a small vicinity around the initial guesses in parameter space and used to compute the low-energy many-body spectra. Out of those guesses, another set of random points is generated, but in a smaller vicinity around the previous set of parameters that yielded a spectrum closest to the atomistic low-energy spectrum. This process is repeated until the difference between the Hubbard-Kanamori and atomistic spectra is below a threshold value and the result is a set of fitted Hubbard-Kanamori parameters. To obtain the fitted parameters, only t, V, and W were varied while the rest of the parameters were held stationary in the genetic algorithm. The set of parameters for this system are given in Table I.

We then compare atomistic, Hubbard-Kanamori, and Heisenberg chain spectra in Fig. 8. Here, the Heisenberg coupling is chosen to be $J_H = \frac{2t^2}{U+\frac{J}{2}-V} = 0.104$ meV.
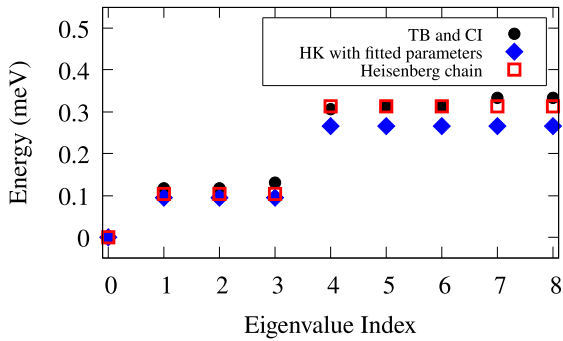
FIG. 8. Comparison between atomistic, Hubbard-Kanamori, and Heisenberg chain spectra.

FIG. 10. Hubbard-Kanamori and Heisenberg low-energy spectrum as a function of total spin S.

The agreement between all three spectra indicates that not only is the parametrized Hubbard-Kanamori model a valid approximation of the atomistic Hamiltonian, but the Hubbard-Kanamori model does in fact exhibit properties of the Heisenberg chain. Though the Heisenberg coupling increases as a function of interdot distance, there is a limit to the magnitude of J_H. This is shown in Fig. 9 with the comparison between overlaps of the Hubbard-Kanamori ground state with the ground states of the Heisenberg Hamiltonian and the molecular Hamiltonian given by

$$H_{\text{Mol}} = t \sum_{\alpha\sigma} c^{\dagger}_{1\alpha\sigma} c_{2\alpha\sigma} + (\text{c.c.}). \qquad (19)$$

In the molecular Hamiltonian, the energy spectrum is dominated by interdot tunneling, with two spin up and down electrons occupying a molecular symmetric p_+ and p_- orbitals instead of forming spin-1 states on each dot. The Heisenberg triplet ground state increasingly becomes a more accurate description of the Hubbard-Kanamori ground state as the interdot distance increases. Conversely, the molecular ground state is a better description for smaller interdot distances when interdot tunneling dominates. At an interdot distance of 10 nm, the Heisenberg ground state accounts for ~70% of the composition of the Hubbard-Kanamori ground

state. Furthermore, at this interdot distance, the system is adequately described in terms of coupled spin-1 particles while simultaneously keeping J_H rather large. It is worth noting that the squared overlaps for a given interdot distance do not sum to unity due to the fact that the Heisenberg and molecular ground states are not orthogonal to each other.

As shown in Fig. 10, the Hubbard-Kanamori and Heisenberg spectra are in agreement with a χ^2 error of ~0.35 meV. This interdot distance yields an effective maximum for the magnitude of the Heisenberg coupling, which in this case is $J_H = 1.096$ meV.

VIII. CONCLUSION

We described here electronic properties of multielectron complexes in InAsP quantum dots in InP nanowires using a combination of a microscopic many-body Hamiltonian based on atomistic tight-binding single-particle states and the configuration interaction approach to electron-electron interactions. We determined the evolution of total spin of the ground state of electronic complexes with electron number and found the synthetic spin-1 state for $N_e = 4$ electrons in a dot. We related the evolution of total spin to the generalized Hund's rule and discussed detection using Coulomb blockade spectroscopy. We extended the microscopic model to two tunnel-coupled quantum dots in a nanowire. We determined the electronic spectra as a function of interdot coupling. We computed the $N_e = 8$ electron complex, with 4 electrons per quantum dot. The low-energy spectra of Hubbard-Kanamori and Heisenberg Hamiltonians were fitted to the low-energy spectra of a microscopic Hamiltonian and understood in terms of two antiferromagnetically coupled spin-1 complexes on each dot. The Hubbard Kanamori parameters and interdot exchange coupling were determined from microscopic calculations. This analysis has shown that a chain of $InAs_{1-x}InP_x$ quantum dots in an InP nanowire can be used to construct a synthetic Heisenberg spin-1 chain described by the Hubbard-Kanamori model. Because of the reduction of the Hilbert space, the Hubbard-Kanamori model will allow for microscopic understanding of macroscopic chains which could be used to construct macroscopic quantum states and topologically protected qubits.
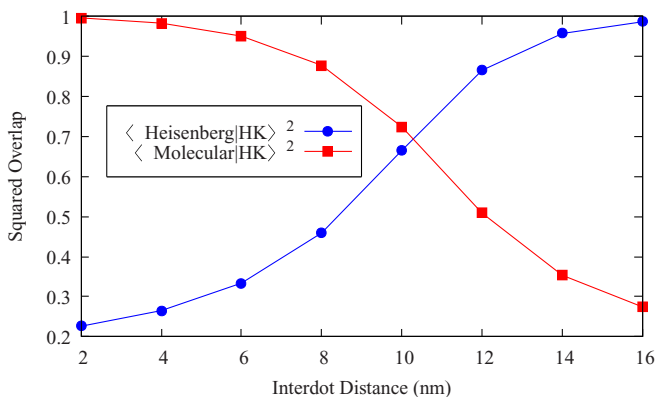

FIG. 9. Comparison between the overlaps of the Hubbard-Kanamori ground state with the Heisenberg $S = 1$ ground state and the molecular ground state.
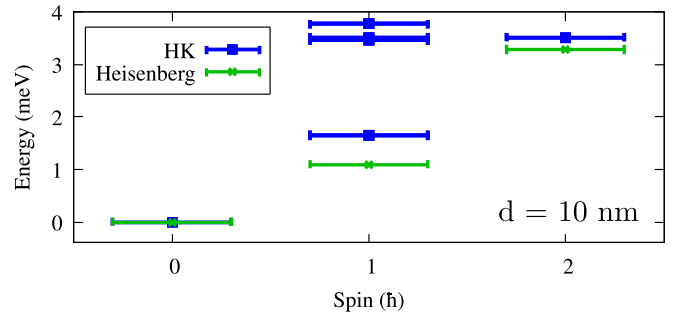
[1] G. W. Bryant, Phys. Rev. Lett. **59**, 1140 (1987).

[2] P. Hawrylak, Phys. Rev. Lett. **71**, 3347 (1993).

[3] R. Ashoori, Nature (London) **379**, 413 (1996).

[4] J. A. Brum and P. Hawrylak, Superlatt. Microstruct. **22**, 431 (1997).

[5] D. Loss and D. P. DiVincenzo, Phys. Rev. A **57**, 120 (1998).

[6] S. Tarucha, D. G. Austing, T. Honda, R. J. van der Hage, and L. P. Kouwenhoven, Phys. Rev. Lett. **77**, 3613 (1996).

[7] M. Ciorga, A. S. Sachrajda, P. Hawrylak, C. Gould, P. Zawadzki, S. Jullian, Y. Feng, and Z. Wasilewski, Phys. Rev. B **61**, R16315 (2000).

[8] R. Hanson, L. P. Kouwenhoven, J. R. Petta, S. Tarucha, and L. M. K. Vandersypen, Rev. Mod. Phys. **79**, 1217 (2007).

[9] C.-Y. Hsieh, Y.-P. Shim, M. Korkusinski, and P. Hawrylak, Rep. Prog. Phys. **75**, 114501 (2012).

[10] B. Jaworowski, N. Rogers, M. Grabowski, and P. Hawrylak, Sci. Rep. **7**, 5529 (2017).

[11] A. West, B. Hensen, A. Jouan, T. Tanttu, C.-H. Yang, A. Rossi, M. F. Gonzalez-Zalba, F. Hudson, A. Morello, D. J. Reilly, and A. S. Dzurak, Nat. Nanotechnol. **14**, 437 (2019).

[12] F. Meier, J. Levy, and D. Loss, Phys. Rev. Lett. **90**, 047901 (2003).

[13] E. Kawakami, P. Scarlino, D. R. Ward, F. R. Braakman, D. E. Savage, M. G. Lagally, M. Friesen, S. N. Coppersmith, M. A. Eriksson, and L. M. K. Vandersypen, Nat. Nanotechnol. **9**, 666 (2014).

[14] B. Jaworowski and P. Hawrylak, Appl. Sci. **9**, 474 (2019).

[15] D. Cogan, O. Kenneth, N. H. Lindner, G. Peniakov, C. Hopfmann, D. Dalacu, P. J. Poole, P. Hawrylak, and D. Gershoni, Phys. Rev. X **8**, 041050 (2018).

[16] O. Benson, C. Santori, M. Pelton, and Y. Yamamoto, Phys. Rev. Lett. **84**, 2513 (2000).

[17] D. Dalacu, K. Mnaymneh, J. Lapointe, X. Wu, P. J. Poole, G. Bulgarini, V. Zwiller, and M. E. Reimer, Nano Lett. **12**, 5919 (2012).

[18] N. Akopian, N. H. Lindner, E. Poem, Y. Berlatzky, J. Avron, D. Gershoni, B. D. Gerardot, and P. M. Petroff, Phys. Rev. Lett. **96**, 130501 (2006).

[19] I. Schwartz, D. Cogan, E. R. Schmidgall, Y. Don, L. Gantz, O. Kenneth, N. H. Lindner, and D. Gershoni, Science **354**, 434 (2016).

[20] Y. Arakawa and H. Sakaki, Appl. Phys. Lett. **40**, 939 (1982).

[21] S. Fafard, K. Hinzer, S. Raymond, M. Dion, J. McCaffrey, Y. Feng, and S. Charbonneau, Science **274**, 1350 (1996).

[22] D. Bimberg, M. Grundmann, F. Heinrichsdorff, N. Ledentsov, V. Ustinov, A. Zhukov, A. Kovsh, M. Maximov, Y. Shernyakov, B. Volovik, A. Tsatsul'nikov, P. Kop'ev, and Z. Alferov, Thin Solid Films **367**, 235 (2000).

[23] M. P. van Kouwen, M. H. M. van Weert, M. E. Reimer, N. Akopian, U. Perinetti, R. E. Algra, E. P. A. M. Bakkers, L. P. Kouwenhoven, and V. Zwiller, Appl. Phys. Lett. **97**, 113108 (2010).

[24] B. Aslan, H. C. Liu, M. Korkusinski, S.-J. Cheng, and P. Hawrylak, Appl. Phys. Lett. **82**, 630 (2003).

[25] M. T. Björk, C. Thelander, A. E. Hansen, L. E. Jensen, M. W. Larsson, L. R. Wallenberg, and L. Samuelson, Nano Lett. **4**, 1621 (2004).

[26] M. P. v. Kouwen, M. E. Reimer, A. W. Hidma, M. H. M. van Weert, R. E. Algra, E. P. A. M. Bakkers, L. P. Kouwenhoven, and V. Zwiller, Nano Lett. **10**, 1817 (2010).

[27] A. Wojs and P. Hawrylak, Phys. Rev. B **53**, 10841 (1996).

[28] A. Wojs and P. Hawrylak, Phys. Rev. B **55**, 13066 (1997).

[29] M. Ediger, G. Bester, A. Badolato, P. M. Petroff, K. Karrai, A. Zunger, and R. J. Warburton, Nat. Phys. **3**, 774 (2007).

[30] G. A. Narvaez and P. Hawrylak, Phys. Rev. B **61**, 13753 (2000).

[31] M. Rontani, F. Rossi, F. Manghi, and E. Molinari, Solid State Commun. **112**, 151 (1999).

[32] L. P. Kouwenhoven, D. G. Austing, and S. Tarucha, Rep. Prog. Phys. **64**, 701 (2001).

[33] M. E. Reimer, G. Bulgarini, A. Fognini, R. W. Heeres, B. J. Witek, M. A. M. Versteegh, A. Rubino, T. Braun, M. Kamp, S. Höfling, D. Dalacu, J. Lapointe, P. J. Poole, and V. Zwiller, Phys. Rev. B **93**, 195316 (2016).

[34] M. Cygorek, M. Korkusinski, and P. Hawrylak, Phys. Rev. B **101**, 075307 (2020).

[35] P. Laferrière, E. Yeung, M. Korkusinski, P. J. Poole, R. L. Williams, D. Dalacu, J. Manalo, M. Cygorek, A. Altintas, and P. Hawrylak, Appl. Phys. Lett. **118**, 161107 (2021).

[36] P. Hawrylak, Phys. Rev. B **60**, 5597 (1999).

[37] S. Raymond, S. Studenikin, A. Sachrajda, Z. Wasilewski, S. J. Cheng, W. Sheng, P. Hawrylak, A. Babinski, M. Potemski, G. Ortner, and M. Bayer, Phys. Rev. Lett. **92**, 187402 (2004).

[38] M. Bayer, O. Stern, P. Hawrylak, S. Fafard, and A. Forchel, Nature (London) **405**, 923 (2000).

[39] M. Bayer, P. Hawrylak, K. Hinzer, S. Fafard, M. Korkusinski, Z. R. Wasilewski, O. Stern, and A. Forchel, Science **291**, 451 (2001).

[40] J. J. Palacios and P. Hawrylak, Phys. Rev. B **51**, 1769 (1995).

[41] M. Korkusiński and P. Hawrylak, Phys. Rev. B **63**, 195311 (2001).

[42] M. Zieliński, Phys. Rev. B **88**, 115424 (2013).

[43] W. Sheng and P. Hawrylak, Phys. Rev. B **72**, 035326 (2005).

[44] M. Zieliński, M. Korkusiński, and P. Hawrylak, Phys. Rev. B **81**, 085301 (2010).

[45] M. Cygorek, M. Otten, M. Korkusinski, and P. Hawrylak, Phys. Rev. B **101**, 205308 (2020).

[46] C. Delerue, M. Lannoo, and G. Allan, Phys. Rev. B **68**, 115411 (2003).

[47] I. Moreels, G. Allan, B. De Geyter, L. Wirtz, C. Delerue, and Z. Hens, Phys. Rev. B **81**, 235319 (2010).

[48] A. Kogan, G. Granger, M. A. Kastner, D. Goldhaber-Gordon, and H. Shtrikman, Phys. Rev. B **67**, 113309 (2003).

[49] F. Simmel, D. Abusch-Magder, D. A. Wharam, M. A. Kastner, and J. P. Kotthaus, Phys. Rev. B **59**, R10441 (1999).

[50] I. Puerto Gimenez, M. Korkusinski, and P. Hawrylak, Phys. Rev. B **76**, 075336 (2007).

[51] M. F. Doty, J. I. Climente, M. Korkusinski, M. Scheibner, A. S. Bracker, P. Hawrylak, and D. Gammon, Phys. Rev. Lett. **102**, 047401 (2009).

[52] B. Jaworowski, Electron Correlations in Topological Flat Bands, Ph.D. thesis, Wrocław University of Science and Technology, 2018.